Am J Physiol Cell Physiol 296: C848–C856, 2009.
First published January 28, 2009; doi:10.1152/ajpcell.00520.2008.

Dynamics of neutrophil extravasation and vascular permeability are uncoupled during aseptic cutaneous wounding

Min-Ho Kim,[1] Fitz-Roy E. Curry,[2] and Scott I. Simon[1]

[1]*Department of Biomedical Engineering, University of California at Davis; and* [2]*Department of Physiology and Membrane Biology, University of California at Davis School of Medicine, Davis, California*

Submitted 9 October 2008; accepted in final form 22 January 2009

Kim MH, Curry FE, Simon SI. Dynamics of neutrophil extravasation and vascular permeability are uncoupled during aseptic cutaneous wounding. *Am J Physiol Cell Physiol* 296: C848–C856, 2009. First published January 28, 2009; doi:10.1152/ajpcell.00520.2008.— Transport of macromolecules and transmigration of leukocytes across vascular endothelium are regulated by a tight molecular junction, but the mechanisms by which these two inflammatory events are differentially controlled in time and magnitude during aseptic cutaneous wounding remain elusive. A real-time fluorescence imaging technique was developed to simultaneously track influx of Alexa 680-labeled albumin and genetically tagged enhanced green fluorescent protein-neutrophils [polymorphonuclear neutrophils (PMN)] within the wound bed. Vascular permeability increased approximately threefold more rapidly than the rate of PMN influx, reaching a maximum at 12 h, on the order of ~0.15% per minute versus ~0.05% per minute for PMN influx, which peaked at 18 h. Systemic depletion of PMN with antibody blocked their extravasation to the wound but did not alter the increase in vascular permeability. In contrast, pretreatment with antiplatelet GPIb decreased permeability by 25% and PMN influx by 50%. Hyperpermeability stimulated by the endothelium-specific agonists VEGF or thrombin at 24 h postwounding was completely inhibited by blocking Rho-kinase-dependent signaling, whereas less inhibition was observed at 1 h and neutrophil influx was not perturbed. These data suggest that in aseptic wounds, the endothelium maintains a tight junctional barrier to protein leakage that is independent of neutrophil transmigration, partially dependent on circulating platelets, and associated with Rho-kinase-dependent signaling.

enhanced green fluorescent protein-polymorphonuclear neutrophils; Rho-kinase; vascular endothelial growth factor; platelets

IN RESPONSE TO TISSUE INJURY, a dynamic process involving release of soluble mediators and recruitment of inflammatory cells initiates and maintains a host response to fight infection and heal injured tissue (35). Early responses essential to this are increased vascular permeability and directed transmigration of neutrophils to the site of injury. Vascular hyperpermeability results in extravasation of fibrinogen and deposition of a fibrin matrix that favors granulation tissue formation and leads to wound healing (4). Neutrophil extravasation into the wound bed provides a critical bacteriocidal function and also serves to reorganize granulation tissue during the process of wound healing (35). Maintaining a precise balance between the rate and extent of neutrophil influx and endothelial cell barrier function is critical to normal wound healing and avoidance of chronic tissue inflammation and scar formation (22, 41, 42).

Numerous studies have demonstrated a neutrophil-dependent alteration in vascular permeability in both in vitro and in vivo experimental models (2, 14, 20, 43, 47, 49). However, many of these studies have relied on the direct activation of neutrophils by addition of chemokines that can signal activation of β_2-integrin binding to endothelial ligands (i.e., ICAM-1) and extracellular matrix molecules (i.e., fibrinogen). This in turn triggers the neutrophil to release permeability-increasing agents in a process intended to mimic the onset of chronic inflammation. In contrast to the established role that neutrophil bacteriocidal and oxidative functions play in the pathogenesis of chronic wounds (29), their function in normal wound healing in the absence of gross infection has been questionable. Indeed, genetic ablation of myeloid cell production using PU.1-null mice was found to not alter tissue repair in aseptic wounds (23). Yet the mechanisms by which permeability and polymorphonuclear neutrophil (PMN) transmigration are functionally linked or differentially regulated in time and magnitude over the dynamics of the inflammatory response under normal wound healing remains elusive and is crucial for understanding the derangements that occur during chronic inflammatory diseases.

To address this issue, we applied a noninvasive whole animal imaging method that simultaneously tracks neutrophil extravasation and protein leakage into a cutaneous wound to correlate the dynamics in neutrophil recruitment and vascular permeability during the initial 24-h inflammatory phase of aseptic wounding. We also examined Rho-kinase-dependent signaling since it is central to regulation of endothelial cytoskeletal contractility (11, 44) and vascular permeability under conditions of inflammation and injury (32). The results show that during the acute response to wounding, neutrophil recruitment is uncoupled from endothelial barrier function for macromolecular transport, which becomes increasingly dependent on Rho-kinase signaling following tissue injury.

MATERIALS AND METHODS

Animals. Mice expressing enhanced green fluorescent protein (EGFP) were generated by cross-breeding 129Sv lys-EGFP mice (generously provided by Dr. Thomas Graf, Albert Einstein College of Medicine, Bronx, NY) with C57BL/6J (Jackson, Bar Harbor, ME) for at least nine generations in the animal facility at University of California at Davis and were housed in the same facility. Mice between 8 and 12 wk of age were used in all the experiments. All animal experiments were approved by the Institutional Animal Care and Use Committee of the University of California at Davis (animal protocol nos. 11777 and 13386).

Address for reprint requests and other correspondence: S. I. Simon, Dept. of Biomedical Engineering, Univ. of California at Davis, 451 E. Health Sciences Dr., Davis, CA 95616 (e-mail: sisimon@ucdavis.edu).

The costs of publication of this article were defrayed in part by the payment of page charges. The article must therefore be hereby marked "*advertisement*" in accordance with 18 U.S.C. Section 1734 solely to indicate this fact.

Skin wound model. Mice were anesthetized with an intraperitoneal injection of ketamine (80 mg/kg)-xylazine (10 mg/kg), and the back skin hair was then removed with a mechanical shaver. After sterilization with 10% wt/vol povidine-iodine and 70% alcohol, 6 mm in diameter circular full-thickness wound was made using a skin biopsy punch (Robbins Instruments, Chatham, NJ).

In vivo fluorescence imaging of EGFP neutrophils and fluorescence-tagged BSA. The in vivo imaging of EGFP neutrophils and fluorescence-tagged BSA appearing on the site of back skin wound was performed using the whole body small animal fluorescence imaging system (Xenogen IVIS 100 system, Xenogen) as described recently (21). Mice were put into the imaging chamber of the system after being anesthetized by ketamine-xylazine. The EGFP-expressing neutrophils within the wound area were visualized using a GFP filter (excitation at 445–490 nm and emission at 515–575 nm) at an exposure time of 1 s. Simultaneous imaging of BSA-Alexa 680 within the wound area was achieved with a CY5.5 filter (excitation at 615–665 nm and emission at 695–770 nm, at an exposure time of 1 s) immediately following the imaging of EGFP-PMNs. In selected experiments, BSA-Alexa 594 within the wound area were imaged using DsRed filter (excitation at 500–550 nm and emission at 575–650 nm, at an exposure time of 1 s). To determine basal vascular permeability in intact skin, BSA-Alexa 680 fluorescence in shaved nonwounded back skin was also imaged using the CY5.5 filter set. Analysis of the images was performed using Live Image Pro. 2.5 software (Caliper Life Sciences), and fluorescence intensities expressed as average radiance (photons per cm^2 per steradian) were measured by drawing a circular region of interest over the entire wound area.

Titration of BSA-Alexa 680. BSA-Alexa 680 was purchased from Invitrogen (Carlsbad, CA; catalog no. A34787, excitation maximum at 679 nm and emission maximum at 702 nm). On the day of the experiment, free Alexa dye within the BSA-Alexa 680 conjugate solution was removed by centrifugation of the 0.5 mg/ml BSA-Alexa 680 solution through a Centrifree (Millipore, Billerica, MA) centrifuge filter. The fluorescence of the ultrafiltrate was checked in the fluorometer and compared with standards prepared from free Alexa dye alone. Repeated centrifugation (e.g., at least 3 times) reduced free dye composition to <0.2%. The concentrated labeled albumin was then diluted with sterile saline. Endotoxin contamination effect within the prepared BSA-Alexa 680 solution was determined in control experiments in which vascular permeability was measured over periods of 100 min after tail-vein injection of BSA-Alexa 680 under superfusion of sterile saline onto the wounded skin. No significant increase in vascular permeability in wounded skin was observed up to 100 min. For the titration experiment, full-thickness wound (6 mm in diameter) was made on top of back skin in EGFP mice using a skin biopsy punch, and different concentrations of BSA-Alexa 680 (0.1, 0.5, and 1.0 mg/ml, dissolved in 100 μl sterile saline) were either applied on to the wounded skin for in vitro titration or injected into the tail vein of separate mice for in vivo titration. Then, BSA fluorescence was determined as a function of BSA concentration.

Spatial mapping of EGFP-PMN and BSA-Alexa 680 fluorescence. To determine spatial localization of EGFP-PMN and BSA-Alexa 680 fluorescence within the circular wound area (6 mm in diameter), images were divided into 96 regions of interest using rectangular segmentation. Fluorescence intensity maps were then obtained for each rectangular segment. Additionally, the 96 rectangular segments were further subdivided into three areas of interest depending on the distance from the center of circular wound (that is, areas of $r = 0–1$, $r = 1–2$, and $r = 2–3$ mm). The average was taken to obtain mean fluorescence intensity, and this value was normalized relative to area $r = 0–1$ mm.

Vascular permeability. Protein extravasation into skin wounds was detected by intravenous tail-vein administration of fluorescence-conjugated albumin as a tracer for vascular leakage across the endothelium. Vascular permeability (P) was quantified using a modification of a previous method developed by Huxley et al. (18) and was calculated by assuming a linear relationship between the measured fluorescence intensity (I) and the concentration of fluorescently conjugated albumin within the wound area. $P = 1/\Delta I(t)\ (dI/dt)\ (r/2)$, where $\Delta I(t)$ is the step increase in fluorescence of tracer molecules due to vascular filling, dI/dt is the rate of albumin extravasation into the surrounding tissue, and r is the average radius of the vessels. During vascular inflammation, the microvascular site of plasma solute leakage is largely from postcapillary venules with diameters ranging between 10 and 40 μm (37). Thus, in this study, median value of vessel radius $r = 12.5$ μm was assumed in calculating vascular permeability. Since plasma concentration of tracer molecule varies with time after injection due to plasma clearance by kidney, liver, and other organs, the vascular filling compartment was defined as a time-dependent function, $\Delta I(t) = \Delta I_o \times f(t)$, where ΔI_o is defined as the initial step increase in fluorescence at $t = 1$ min following injection of tracer molecules and $f(t)$ was determined by fitting the data of plasma concentration of tracer molecule to a single exponential decay function $f(t) = a \times \exp(-1/k \times t) + b$. To estimate this, we measured the clearance of Alexa 680-BSA from blood samples collected at 5, 30, 60, and 90 min following tail-vein injection. The constants a and b were found to have values 0.34 and 0.65, respectively, and the time constant $k = 6 \times 10^3$ s. The accuracy of the exponential decay estimate was tested by measuring permeability of both Alexa 680-BSA at 60 min and that of second tracer, Alexa 594-BSA, injected 45 min later. This estimation technique predicts total apparent permeability and does not discriminate between the convective versus diffusive contributions to shifts in the permeability coefficient.

Experimental protocols. The permeability of albumin within the vasculature of cutaneous wounds was measured during the early (1 h) and late phase (24 h) of the inflammatory response by injecting fluorescent Alexa 680-conjugated BSA into the mouse tail vein at each phase and quantifying the time-dependent change in fluorescence intensity. For early phase measurement, BSA-Alexa 680 (0.5 mg/ml, 100 μl) was injected within 30 min of skin wounding, and basal vascular permeability was determined under topical superfusion of saline to the wounded area for 30 min. The reactive response of vascular permeability was determined by topically superfusing 100 μl of either VEGF (1,000 ng/ml, Sigma-Aldrich, St. Louis, MO) or thrombin (5 U/ml, Sigma-Aldrich) to the wound following 30 min of baseline measurement. To investigate the effect of Rho-kinase inhibition on VEGF-induced response, Y-27632 (50 μM, Sigma-Aldrich) was pretreated for 40 min to the wound and then VEGF was topically applied in the presence of Y-27632.

For measurement of late phase response, mice were maintained in the animal housing facility for 24 h postwounding, and the identical experimental procedure as the early phase measurement was performed under treatment of saline, thrombin, VEGF, or Y-27632. To investigate the effect of proteinase-activated receptor-1 (PAR-1) activation on vascular permeability, PAR-1 agonist peptide (PAR-1 AP, $SFLLRN\text{-}NH_2$, 5 μM, Sigma-Aldrich) was topically superfused into the wound following 30 min of baseline measurement. The depletion of circulating PMNs and platelets was achieved by pretreatment (intraperitoneal injection) with either anti-Gr-1 antibody (0.1 mg, BD Biosciences, San Diego, CA) for PMN depletion or anti-CD41 antibody for platelet depletion (0.1 mg, BD Biosciences) at 1 h before skin wounding. Then, the effect of depletion of circulating PMNs or platelets on the responsiveness to thrombin, VEGF, PAR-1 AP, or saline for control was examined by topically supefusing these agents to the wound. The efficacy of Gr-1 and CD41 antibody in depleting >90% of PMNs and platelets was confirmed by differential blood counts (data not shown).

In selected experiments, kinetic data of vascular permeability were also obtained at time points of 6 h, 12 h, and 18 h postwounding.

Statistical analysis. Data analysis was performed using GraphPad Prism version 4.0 software (GraphPad Software, San Diego, CA). Statistical tests among multiple groups were analyzed using one-way

ANOVA followed by Tukey's posttest for secondary analysis for significance. Statistical significance between two groups was determined by two-tailed unpaired *t*-tests. *P* values of <0.05 were considered statistically significant.

RESULTS

Noninvasive imaging of vascular permeability. To measure the extravasation of proteins from the vasculature during cutaneous wounding, Alexa 680-conjugated BSA was injected into the mouse tail vein during the early (1 h) and late (24 h) phases of the inflammatory response (Fig. 1*A*). Fluorescent albumin accumulated toward the center of the wound and not along the wound margin, indicating a minor contribution from bleeding of severed vessels, which was efficiently staunched by coagulation soon after wounding. A linear correlation was confirmed between fluorescence intensity and the concentration of BSA-Alexa 680 exogenously applied directly into the wound ($r^2 = 0.9579$ and $P < 0.0001$; Fig. 1*B*). Likewise, a linear correlation was observed in response to increasing concentrations of BSA-Alexa 680 detected in the wound bed within minutes of venous injection ($r^2 = 0.8423$ and $P < 0.0001$; Fig. 1*C*). Vascular permeability was measured by quantifying the time-dependent change in fluorescence signal of tracer BSA in both vascular [$\Delta I_o(t)$] and tissue compartments [I(t)] and applying a kinetic model that estimates transport across the vessel wall, as described in detail in MATERIALS AND METHODS. Vascular filling (ΔI_o) was estimated from the step increase in fluorescence intensity within 1 min of tail-vein injection of BSA-Alexa 680 (Fig. 1*D*). A second injection of BSA-Alexa 594 was applied 40 min later and confirmed that the signal from vascular filling remained constant. Vascular permeability was computed from dI/d*t* and the kinetic model and found to be $\sim 2.4 \times 10^{-7}$ cm/s for albumin at 1 h postwounding (Fig. 1*E*). This value was not significantly different from the basal value detected in nonwounded intact skin ($1.63 \pm 0.26 \times 10^{-7}$ cm/s, $P > 0.05$ vs. 1 h). Within 24 h of wounding, a time-dependent increase in vascular permeability was detected in that the BSA-Alexa 680 permeability coefficient increased approximately threefold ($2.40 \pm 0.43 \times 10^{-7}$ cm/s at 1 h vs. $6.25 \pm 0.93 \times 10^{-7}$ cm/s at 24 h; Fig. 1*E*). The measured solute permeability coefficients at both 1 and 24 h postwounding were also found to be independent of the venous

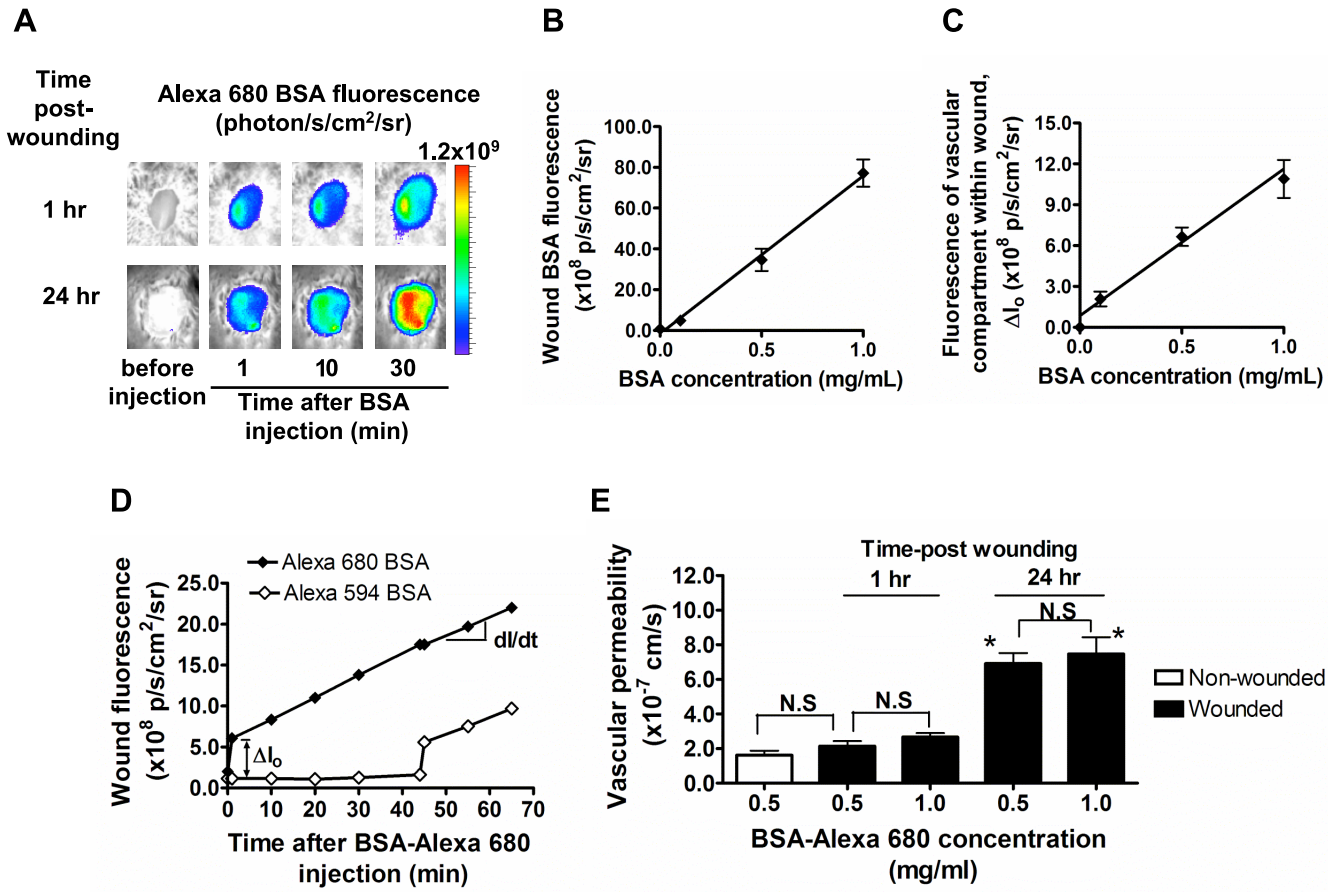

Fig. 1. Real-time detection of vascular permeability using fluorescent albumin. *A*: noninvasive fluorescence imaging of BSA-Alexa 680 before and after intravenous (iv) injection at early (1 h) and late (24 h) phase after skin wound. p/s/cm²/sr, photons per square centimeter per steradian. *B*: topical application of BSA-Alexa 680 directly into the wound. Fluorescence intensity within wound area was measured as a function of BSA titrated into wound. *C*: in vivo titration of BSA-Alexa 680. BSA-Alexa 680 was injected via tail vein (iv), and fluorescence intensity of BSA within vascular compartment (I_o, BSA fluorescence measured 1 min after injection) was measured as a function of injected BSA concentration. *D*: representative time course of BSA fluorescence within wound. The effect of plasma clearance of circulating BSA-Alexa 680 on permeability measurement was assessed by comparing the response obtained by second dye, in which Alexa 594 BSA was injected 45 min after Alexa 680 BSA injection. *E*: comparison of baseline vascular permeability in nonwounded intact skin and wounded skin. Vascular permeability is also shown as a function of BSA concentration (0.5 and 1.0 mg/ml) in wounded skin at both 1 h and 24 h postwounding. NS, not significant. $^*P < 0.05$ with respect to 1 h group; $n = 3$ to 4 mice in each group.

concentration of BSA injected. The permeability coefficient estimated using BSA-Alexa 680 ($5.58 \pm 0.35 \times 10^{-7}$ cm/s) after 60 min of injection at 24 h postwounding was within ~10% of the value of BSA-Alexa 594 ($6.17 \pm 0.22 \times 10^{-7}$ cm/s) at the same time point. Taken together, these data indicate that detection of albumin transport was independent of the fluorophore wavelength or concentration perfused and provided a faithful measure of vascular permeability into the wound bed.

We next examined the role of VEGF receptor-2 in endothelium-specific regulation of permeability. VEGF165 was topically superfused into the wound bed during the early and late phases of wounding or subcutaneously injected into intact skin. The baseline rate of albumin leakage was not significantly different between nonwounded and wounded skin at 1 h, but it increased by approximately threefold at 24 h (Fig. 2). Within 10 min of VEGF application, a rapid increase in vascular permeability was detected, which decreased back to baseline values within 20 min in both intact and wounded skin. This rapid and transient increase in response to VEGF is consistent with a previous report in which permeability was measured in single vessels (3) and indicates that the endothelium can rapidly recover barrier function following acute injury. However, baseline barrier function following 24 h of wounding adjusted to significantly higher baseline permeability.

Vascular permeability is independent of neutrophil recruitment, but partially dependent on platelets. We next examined the role of neutrophils in the regulation of vascular permeability over 24 h of the inflammatory phase of wounding. Green fluorescent neutrophils were detected in the wounds of mice containing the lysozyme-EGFP transgene, which enabled simultaneous analysis of the spatial and temporal distribution with BSA-Alexa 680 fluorescence. Although both permeability and neutrophil influx increased over 24 h, permeability rose more rapidly, reaching a maximum ~6 h before neutrophil influx achieved its peak level at 18 h (Fig. 3*A*). To determine whether these two events are coupled or differentially regulated over the time course of wounding, image analysis was applied to map the intensity of extravasated BSA and PMN. EGFP-PMN fluorescence increased to a maximum in intensity along the wound edge (Fig. 3, *B* and *C*). This is consistent with our previous report that confirmed these PMN to be Gr-1 positive and accumulate in numbers up to sixfold greater than the circulating count (21). In contrast, BSA-Alexa 680 fluorescence was highest at the wound center and decreased in intensity toward the wound periphery (Fig. 3, *B* and *C*). Discrimination between changes in permeability and neutrophil infiltration was also supported by experiments in which neutrophils were depleted by intraperitoneal injection of Gr-1 antibody. This treatment effectively decreased the systemic neutrophil count by ~95%, which correlated with inhibition of EGFP-PMN influx by ~90% (Fig. 3, *D* and *E*). Under these conditions, vascular permeability at 24 h was not significantly different from the wounded control mice that exhibited normal neutrophil influx. Collectively, spatial mapping analysis and neutrophil depletion clearly reveal an uncoupling between the rapid increase in vascular permeability and the migration of EGFP-PMN into the wound bed.

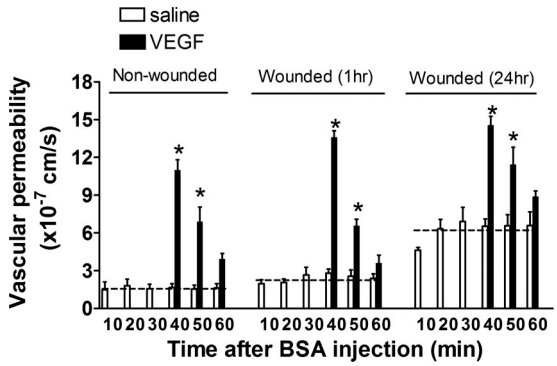

Fig. 2. Vascular permeability in response to VEGF. Time course is shown of vascular permeability in response to VEGF at nonwounded intact skin and at early (1 h) and late (24 h) phase following skin wounding. VEGF was topically treated onto wound area at 30 min following BSA-Alexa 680 injection. Dotted lines indicate mean values of basal permeability (saline control) in each group. *$P < 0.05$ with respect to saline control group; $n = 4$ to 6 mice in each group.

Since cutaneous wounding triggers aggregation and activation of platelets that superpose with endothelial activation, we next examined whether platelets are involved in mediating neutrophil influx and vascular permeability at 24 h of wounding. Antibody depletion of circulating platelets was achieved by intraperitoneal injection of monoclonal antibody specific for CD41 (39), which significantly depleted circulating platelets by ~90% as confirmed by systemic blood counts (data not shown). Under these conditions, the vascular permeability dropped by 40% of the untreated control at 24 h (Fig. 3*E*). In addition, platelet depletion reduced EGFP-PMN infiltration by ~50% (Fig. 3, *D* and *E*). These data reveal a significant influence of activated platelets on endothelial barrier function and are consistent with the well-reported inflammatory effect of platelets on the endothelium (9).

Respective roles of platelet and endothelial activation in vascular permeability. To further assess the respective roles of platelet and endothelial activation on vascular permeability, we applied cell-specific agonists to wounds at the early and late phases of inflammation. Thrombin is a potent serine protease and regulates platelet aggregation and endothelial barrier function by activating PAR (7). Potent activation through thrombin appears to require prior inflammatory challenge as previously observed in single microvessel perfusion studies (8). This was confirmed in this mouse wound model in that topical application of thrombin to the wound at 24 h induced a rapid increase in permeability, whereas no significant increase was detected at 1 h of wounding (Fig. 4). As with VEGF, hyperpermeability was reversible within 20 min and was not altered by neutrophil depletion with Gr-1, suggesting that thrombin acted specifically on platelets and endothelium. We next examined the role of a specific thrombin receptor, PAR-1, that is upregulated on injured endothelium but not expressed on murine platelets (7). We tested whether PAR-1 upregulation was linked to differential sensitivity of thrombin responsiveness by superfusing the wound with a high-affinity peptide agonist to PAR-1 receptor (PAR-1-AP, SFLLRN-NH_2). Addition of PAR-1-AP increased permeability to a similar extent as thrombin at 24 h, but like thrombin had little effect at 1 h (Fig. 4*B*). To determine the role of platelets, mice were again treated with anti-CD41 and activated with thrombin. Depletion of platelets inhibited the thrombin-activated permeability increase by ~40%, dropping it almost to the baseline at 24 h (Fig. 4*B*).

Topical administration of thrombin or PAR-1 AP did not stimulate an increase in the level of PMN influx above that

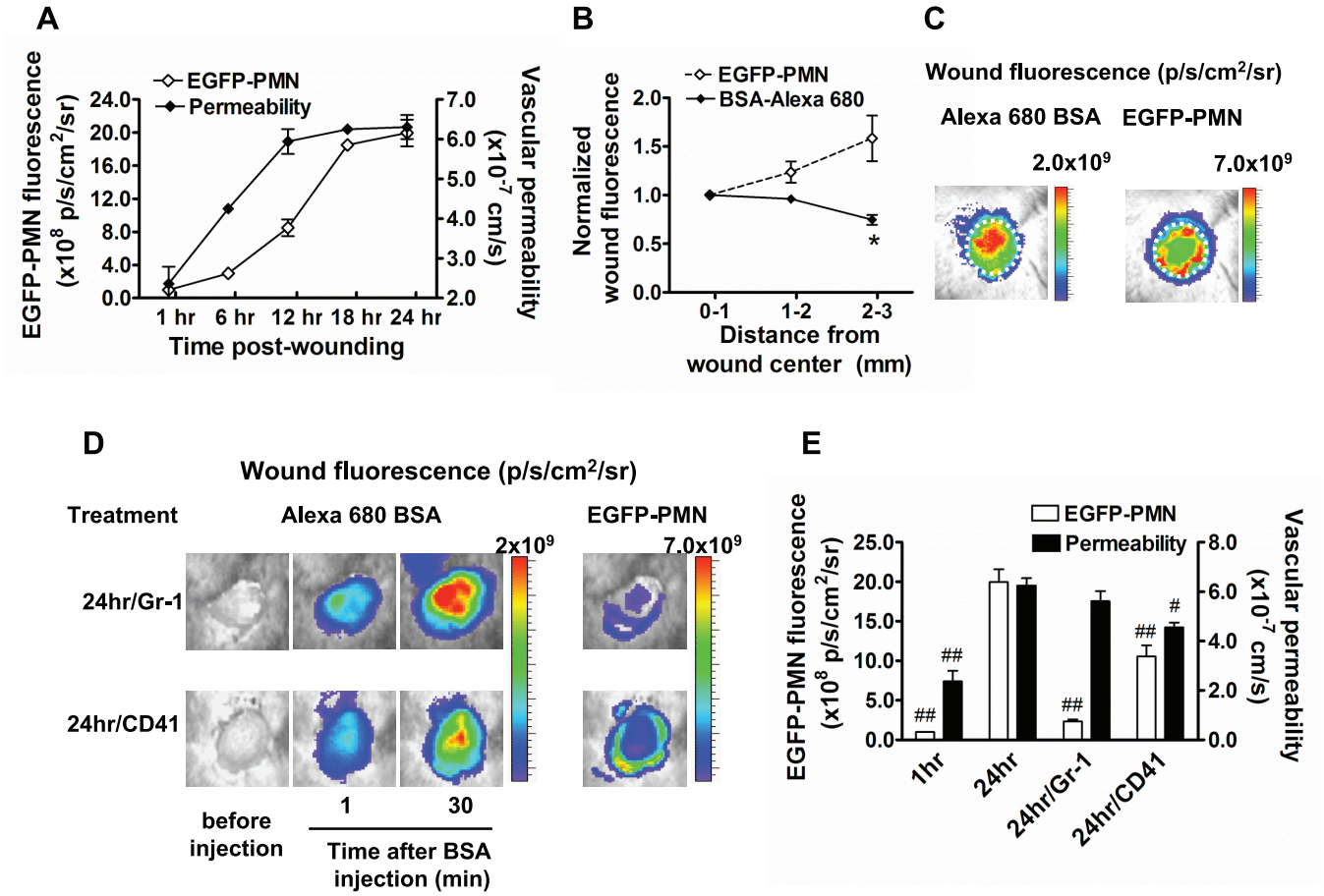

Fig. 3. Spatiotemporal analysis of vascular permeability and polymorphonuclear neutrophil (PMN) influx in response to immunodepletion. *A*: kinetics of enhanced green fluorescent protein (EGFP)-PMN infiltration and vascular permeability. *B* and *C*: spatial mapping of EGFP-PMN and BSA-Alexa 680 fluorescence. The average fluorescence intensities of EGFP-PMN and BSA-Alexa 680 are quantified as a function of distance from wound center, normalized to the averaged value at region $r = 0$–1 mm, and colorized on the basis of intensity. Regions of intense BSA leakage (wound center, $r = 0$–1 mm region) is distinct from greatest density of PMN influx (wound edge, $r = 2$–3 mm region). *$P < 0.05$ with respect to EGFP-PMN group. *D*: representative fluorescent image of EGFP-PMN and BSA-Alexa 680 under depletion of circulating PMNs (Gr-1) and platelets (CD41) within wound at 24 h postwounding. *E*: effect of PMN and platelet depletions on vascular permeability. #$P < 0.05$ and ##$P < 0.01$ with respect to 24 h group; $n = 4$ to 8 mice in each group.

due to wounding alone (Fig. 4*C*). It was confirmed that this was not due to an inability of the agonists to access the vascular compartment and activate neutrophil arrest and transmigration by topically superfusing the strong chemoattractant macrophage inflammatory protein-1α (MIP-1α) and following the time course of EGFP-PMN influx. EGFP-PMN fluorescence in the wound rose by ~40% after 40 min of MIP-1α superfusion, a statistically significant increase over the ~10% rise observed for the saline control group (data not shown). These data reveal a neutrophil- independent and platelet-dependent increase in vascular permeability associated with an upregulation in thrombin receptor responsiveness of the endothelium.

Rho-kinase-dependent signaling regulates vascular permeability during wounding. It has been reported that VEGF-stimulated paracellular transport processes involves cytoskeletal contractility signaled via RhoA (36, 48), as well as RhoA-independent alterations in the adherence junction associated with VE-cadherin internalization (15). It is well established that endothelial permeability is rapidly signaled via a RhoA/Rho-kinase pathway as studied in in vitro models of inflammation (24, 44) and in the pathogenesis of chronic diseases in vivo (27, 32). This motivated the last set of experiments in which we inhibited Rho-kinase and examined the inflammatory response. Wounds were superfused with Y-27632 (e.g., 50 μM) for 40 min, a specific pharmacological inhibitor of Rho-kinase, in the presence and absence of endothelial specific agonists added at 1 and 24 h. Depicted in Fig. 5*A* are the effects of Y-27632 added directly to wounds for 40 min at 24 h following wounding. Rho-kinase inhibition did not significantly alter neutrophil influx, while permeability was inhibited by 70% under these same conditions (Fig. 5*B*). In response to VEGF stimulation at 24 h of wounding, Y-27632 attenuated ~75% of the permeability increase, whereas at 1 h of wounding there was only a ~35% inhibition of VEGF stimulation and no drop from the saline control level at 1 h (Fig. 5, *C* and *D*). Since there was no hyperpermeability response to thrombin at the 1-h time point, stimulation was assessed only at the 24-h time point in the presence or absence of Rho-kinase inhibitor. Thrombin-stimulated vascular permeability in the presence of Y-27632 was completely inhibited (Fig. 5, *C* and *D*). These data clearly show that a Rho-kinase signaling pathway plays an increasing role in endothelial hyperpermeability over time of wounding and the response to inflammatory agonists, while

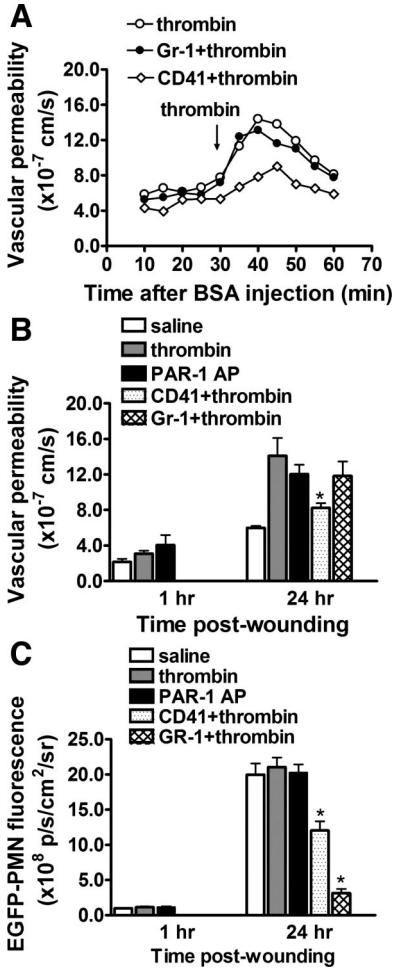

Fig. 4. Thrombin-induced permeability is dependent on platelets and proteinase-activated receptor-1 (PAR-1) expression, but not on PMN recruitment. *A*: representative time course of thrombin-induced vascular permeability under control, PMN depletion with Gr-1 antibody, and platelet depletion with CD41 antibody at 24 h postwounding. Responses are representative of 5 to 7 mice. *B*: effects of PAR-1 expression, PMN depletion, and platelet depletion on thrombin-induced vascular permeability were investigated. Vascular permeability is increased by thrombin and PAR-1-activating peptide (AP) only after 24 h skin wounding. Thrombin-induced response was attenuated by platelet depletion but is not altered by PMN depletion. *C*: effects of thrombin and PAR-1-activating peptide on EGFP-PMN infiltration. $*P < 0.05$ with respect to thrombin group; $n = 5$ to 9 in each group.

neutrophil recruitment is unaffected by blocking Rho-kinase within the wound bed.

DISCUSSION

Maintenance of a tight endothelial junction is necessary to regulate transport of fluid and macromolecules and neutrophil recruitment into injured tissue, while simultaneously providing a barrier against systemic invasion by bacteria and other pathogens. High-resolution whole animal imaging revealed an uncoupling between neutrophil recruitment and vascular permeability during the early inflammatory phase of aseptic cutaneous wounding in that the latter reached a maximum at least 6 h before the peak of neutrophil influx to the wound bed. These two inflammatory events were spatially distinct and differentially regulated because the basal increase in permeability in response to wounding was unperturbed by removal of circulating neutrophils, while it was partially diminished when platelets were depleted. Furthermore, we demonstrated that the increase in vascular permeability over time of wounding was largely mediated by Rho-kinase-dependent signaling, as was the marked potentiation of the response to the endothelium-specific agonists VEGF and thrombin. Our data demonstrate that the endothelium is the primary regulator of fluid and protein transport, which is not altered by the presence of robust neutrophil recruitment.

In the current study, a real-time noninvasive fluorescence imaging technique was introduced that provides continuous detection of the influx of EGFP-PMN and Alexa 680 conjugated albumin into the wound bed. The Xenogen imaging system used in this study can resolve as few as 3.5×10^4 EGFP-PMNs/mm^2 recruited into the wound bed (21) and proved to be highly sensitive in detection of small shifts in vascular permeability. A remarkable finding was that at 1 h postwounding, albumin transport across the vasculature of the wound was within onefold of that measured in unperturbed skin. The increase in permeability ($\sim 2.4 \times 10^{-7}$ cm/s) was slightly lower but on par with that measured during inflammation of single postcapillary venules (e.g., $\sim 4.9 \times 10^{-7}$ cm/s on 25- to 40-μm venules) as detected with a Texas Red-conjugated albumin (30). The acute response at 1 h of wounding was relatively small compared with the approximately threefold increase detected at 24 h, and the approximately sixfold increase stimulated by VEGF or thrombin. We conclude that the endothelium maintains a tight junction and an intact barrier function over hours of skin wounding, yet remains highly responsive to endothelial specific inflammatory stimuli.

Genetic tagging of neutrophils allowed us to simultaneously follow the dynamics of neutrophil recruitment along with vascular permeability. We observed that the kinetics in neutrophil influx and the reversible hyperpermeability response were distinct. Over the initial 12 h, permeability increased approximately threefold more rapidly than the rate of PMN influx, on the order of ~0.15% per minute versus ~0.05% per minute for PMN influx. Moreover, spatial detection of albumin transport revealed it was most intense toward the center of the wound bed, spatially distinct from the location of intense EGFP-PMN influx at the periphery. Immunodepletion of neutrophils with antibody effectively blocked their influx to the wound but did not alter the hyperpermeability response, which was partly inhibited by the immunodepletion of platelets.

The observed uncoupling of neutrophil and macromolecular transport across endothelium is in apparent conflict with previous studies that demonstrate a primary role of neutrophils in altering vascular permeability (2, 14, 20, 43, 47, 49). We believe that this difference can be attributed to variation in the extent of neutrophil activation in aseptic versus infected wounds. In the absence of gross infection, neutrophils are activated by chemotactic agents that efficiently cause it to arrest and transmigrate with little activation of neutrophil degranulation and production of reactive oxygen species. In this context, we have recently reported that boosting the rate and extent of neutrophil influx to a cutaneous wound was critical for clearing gram-positive bacteria. However, it did not alter the efficiency of wound healing and closure, nor the concomitant reduction in neutrophil numbers within the wound over time (21). During sepsis, however, mediators released by activated neutrophils through chemokine signaling (43, 47, 49)

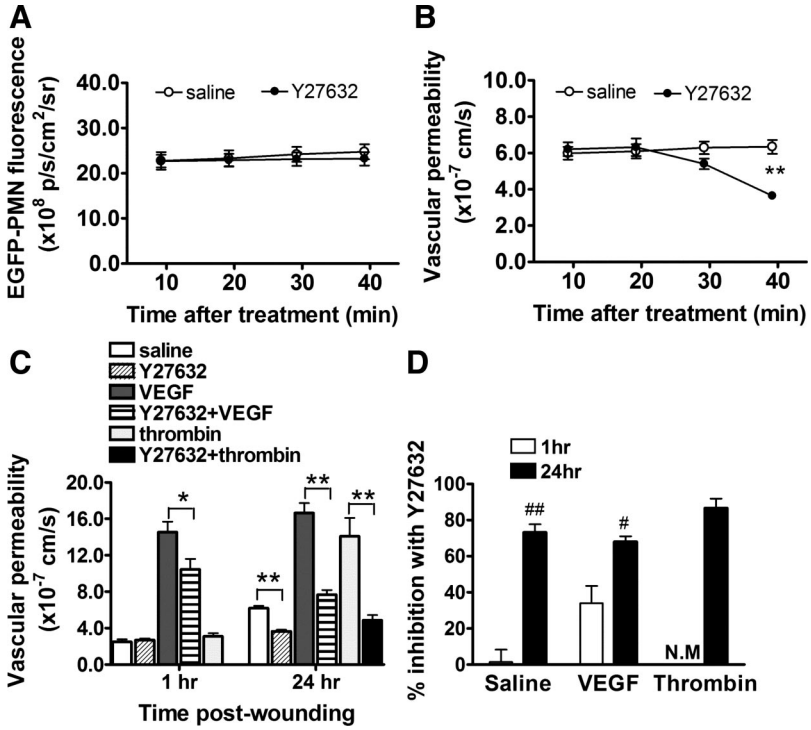

Fig. 5. Rho-kinase inhibition reduces thrombin- and VEGF-stimulated vascular hyperpermeability. *A*: effect of Rho-kinase inhibition with Y-27632 on time course of EGFP-PMN infiltration within wound at 24 h postwounding. *B*: effect of Rho-kinase inhibition with Y-27632 on time course of basal vascular permeability within wound at 24 h postwounding. *C*: vascular permeability at 1 h and 24 h postwounding and effect of Rho-kinase inhibition with Y-27632 on basal, thrombin-, and VEGF-induced vascular permeability. *D*: relative extent of inhibition of vascular permeability with Y-27632 treatment. NM, not measured. $*P < 0.05$ and $**P < 0.01$ between groups and $\#P < 0.05$ and $\#\#P < 0.01$ with respect to 1 h group; $n = 5$ to 7 mice in each group.

and β_2-integrin engagement (2, 14, 20) can trigger alterations in vascular permeability that contribute to vascular injury. For example, in chronic wounds, unresolved inflammation is associated with excessive recruitment of neutrophils, phagocytic activation, and a delay in apoptosis that can prolong the inflammatory response, leading to neutrophil-dependent tissue edema and injury (20, 29, 33).

In contrast to the absence of a direct effect of depleting neutrophils, systemic depletion of platelets with anti-GPIb antibody revealed a cooperative role in neutrophil extravasation and basal and thrombin-induced hyperpermeability. Since PAR-1 receptor signaling reproduced this activation and is endothelium specific, we conclude that the attenuated response by platelet depletion was the result of direct endothelial activation. Platelet adhesion to wounded endothelium can trigger thrombotic activation at the site of injury, which may elicit endothelial activation by upregulating RhoA/Rho-kinase activity in a paracrine-dependent manner (7, 46).

It is well reported that regulation of endothelial permeability is in part signaled via receptor-mediated Ca^{2+} activation of myosin light chain kinase (MLCK) and Rho-kinase activation that in turn mediates cell contractility and the integrity of adherens junctions (38). We have provided evidence here that Rho-kinase-dependent signaling regulates not only the threefold increase in basal permeability over 24 h postwounding, but also the agonist-induced (e.g., thrombin and VEGF) shifts in permeability in wounded skin tissue. The increased dependence on Rho-kinase signaling after 24 h compared with 1 h is consistent with previous reports from our laboratory that Rho-dependent contractile pathways do not contribute significantly to acute increases in permeability by agents such as platelet-activating factor and bradykinin in intact microvessels with no prior exposure to injury (1). The result is also consistent with previous reports of Rho-kinase-dependent regulation in sustained MLC phosphorylation and subsequent cell contractility (25, 40). Indeed, greater than 50% of molecular transport occurs through leaky endothelial junctions that are regulated via agonist receptor-mediated and Rho-kinase-dependent signaling (19, 45). This is consistent with the level of inhibition observed in our studies upon superfusion of Y-27632. It should be noted that Ca^{2+}-dependent MLCK is also involved in the transient opening of adherence junctions during neutrophil diapedesis (13, 17, 31) and that these MLCK- and Rho-dependent pathways may regulate at least part of transient acute shifts in barrier function following wounding.

However, this signaling pathway appears to be unperturbed by robust neutrophil extravasation since Rho-kinase inhibition with Y-27632 did not alter the extent of neutrophil accumulation in the wound. It has previously been reported that greater than 70% of PMNs transmigrate at tricellular endothelial tight junctions (5, 16). A remarkable finding in these studies was that PMN transmigration did not involve significant disruption of tight junctions, while permeability-increasing agents such as histamin can induce a widespread disruption in barrier function. Facilitating this is a tightly regulated multistep process, which includes not only the transient opening of adherence junctions mediated by Ca^{2+} activation of MLCK, but also the coordinated participation of junctional molecules such as platelet/endothelial adhesion molecule (PECAM) and junctional adhesion molecules (JAMs) that form homophilic bonds, thereby maintaining a tight seal during the transmigration process (10, 22, 41, 42). Cooperativity between the endothelium and neutrophil is evidenced by formation of a transmigratory cup that encapsulates the neutrophil and forms a tight membrane seal during transmigration (6, 28). This process occurs very quickly within minutes, and adherence junctions are rapidly reassembled afterward. Immunofluorescence imaging of this process employing VE-cadherin-GFP transfected

endothelium has revealed its rapid and transient displacement from cell junctions within 5 min of neutrophil transmigration (34). We conclude that during the acute inflammatory response, neutrophil influx is essentially uncoupled from the regulation in endothelial barrier function for macromolecular transport. It should be noted that this balance may become altered during chronic inflammation that is defined by significantly heightened levels of influx, delayed neutrophil apoptosis, unresolved wound closure, and/or unchecked bacterial colonization (12, 26).

In summary, we demonstrated that robust neutrophil recruitment into an aseptic cutaneous wound does not alter the autoregulation of endothelial barrier function for macromolecular transport that is controlled by Rho-kinase-dependent signaling. Our data suggest that Rho-kinase regulation of endothelial contractility and/or intracellular tight junctions in response to tissue injury and soluble agonists are central to control of fluid and macromolecular transport even under dynamic inflammatory microenvironments rich in infiltrated neutrophils and platelets.

ACKNOWLEDGMENTS

We thank Dr. Thomas Graf for generously providing the EGFP-lysozyme transgenic mice.

GRANTS

S. I. Simon is supported by National Institutes of Health (NIH) Grant AI-42794 and F.-R. E. Curry is supported by NIH Grant HL-28607.

REFERENCES

1. **Adamson RH, Zeng M, Adamson GN, Lenz JF, Curry FE.** PAF- and bradykinin-induced hyperpermeability of rat venules is independent of actin-myosin contraction. *Am J Physiol Heart Circ Physiol* 285: H406–H417, 2003.
2. **Arfors KE, Lundberg C, Lindbom L, Lundberg K, Beatty PG, Harlan JM.** A monoclonal antibody to the membrane glycoprotein complex CD18 inhibits polymorphonuclear leukocyte accumulation and plasma leakage in vivo. *Blood* 69: 338–340, 1987.
3. **Bates DO, Curry FE.** Vascular endothelial growth factor increases microvascular permeability via a Ca^{2+}-dependent pathway. *Am J Physiol Heart Circ Physiol* 273: H687–H694, 1997.
4. **Brown LF, Yeo KT, Berse B, Yeo TK, Senger DR, Dvorak HF, van de Water L.** Expression of vascular permeability factor (vascular endothelial growth factor) by epidermal keratinocytes during wound healing. *J Exp Med* 176: 1375–1379, 1992.
5. **Burns AR, Bowden RA, MacDonell SD, Walker DC, Odebunmi TO, Donnachie EM, Simon SI, Entman ML, Smith CW.** Analysis of tight junctions during neutrophil transendothelial migration. *J Cell Sci* 113: 45–57, 2000.
6. **Carman CV, Springer TA.** A transmigratory cup in leukocyte diapedesis both through individual vascular endothelial cells and between them. *J Cell Biol* 167: 377–388, 2004.
7. **Coughlin SR.** Thrombin signalling and protease-activated receptors. *Nature* 407: 258–264, 2000.
8. **Curry FE, Zeng M, Adamson RH.** Thrombin increases permeability only in venules exposed to inflammatory conditions. *Am J Physiol Heart Circ Physiol* 285: H2446–H2453, 2003.
9. **Davi G, Patrono C.** Platelet activation and atherothrombosis. *N Engl J Med* 357: 2482–2494, 2007.
10. **Dejana E.** Endothelial cell-cell junctions: happy together. *Nat Rev Mol Cell Biol* 5: 261–270, 2004.
11. **Dudek SM, Garcia JG.** Cytoskeletal regulation of pulmonary vascular permeability. *J Appl Physiol* 91: 1487–1500, 2001.
12. **Edwards R, Harding KG.** Bacteria and wound healing. *Curr Opin Infect Dis* 17: 91–96, 2004.
13. **Garcia JG, Verin AD, Herenyiova M, English D.** Adherent neutrophils activate endothelial myosin light chain kinase: role in transendothelial migration. *J Appl Physiol* 84: 1817–1821, 1998.
14. **Gautam N, Herwald H, Hedqvist P, Lindbom L.** Signaling via beta(2) integrins triggers neutrophil-dependent alteration in endothelial barrier function. *J Exp Med* 191: 1829–1839, 2000.
15. **Gavard J, Gutkind JS.** VEGF controls endothelial-cell permeability by promoting the beta-arrestin-dependent endocytosis of VE-cadherin. *Nat Cell Biol* 8: 1223–1234, 2006.
16. **Gopalan PK, Burns AR, Simon SI, Sparks S, McIntire LV, Smith CW.** Preferential sites for stationary adhesion of neutrophils to cytokine-stimulated HUVEC under flow conditions. *J Leukoc Biol* 68: 47–57, 2000.
17. **Huang AJ, Manning JE, Bandak TM, Ratau MC, Hanser KR, Silverstein SC.** Endothelial cell cytosolic free calcium regulates neutrophil migration across monolayers of endothelial cells. *J Cell Biol* 120: 1371–1380, 1993.
18. **Huxley VH, Curry FE, Adamson RH.** Quantitative fluorescence microscopy on single capillaries: α-lactalbumin transport. *Am J Physiol Heart Circ Physiol* 252: H188–H197, 1987.
19. **Jacobson JR, Barnard JW, Grigoryev DN, Ma SF, Tuder RM, Garcia JG.** Simvastatin attenuates vascular leak and inflammation in murine inflammatory lung injury. *Am J Physiol Lung Cell Mol Physiol* 288: L1026–L1032, 2005.
20. **Kaslovsky RA, Horgan MJ, Lum H, McCandless BK, Gilboa N, Wright SD, Malik AB.** Pulmonary edema induced by phagocytosing neutrophils. Protective effect of monoclonal antibody against phagocyte CD18 integrin. *Circ Res* 67: 795–802, 1990.
21. **Kim MH, Liu W, Borjesson DL, Curry FR, Miller LS, Cheung AL, Liu FT, Isseroff RR, Simon SI.** Dynamics of neutrophil infiltration during cutaneous wound healing and infection using fluorescence imaging. *J Invest Dermatol* 128: 1812–1820, 2008.
22. **Ley K, Laudanna C, Cybulsky MI, Nourshargh S.** Getting to the site of inflammation: the leukocyte adhesion cascade updated. *Nat Rev Immunol* 7: 678–689, 2007.
23. **Martin P, D'Souza D, Martin J, Grose R, Cooper L, Maki R, McKercher SR.** Wound healing in the PU.1 null mouse–tissue repair is not dependent on inflammatory cells. *Curr Biol* 13: 1122–1128, 2003.
24. **Mehta D, Malik AB.** Signaling mechanisms regulating endothelial permeability. *Physiol Rev* 86: 279–367, 2006.
25. **Miyazaki K, Yano T, Schmidt DJ, Tokui T, Shibata M, Lifshitz LM, Kimura S, Tuft RA, Ikebe M.** Rho-dependent agonist-induced spatiotemporal change in myosin phosphorylation in smooth muscle cells. *J Biol Chem* 277: 725–734, 2002.
26. **Ocana MG, Asensi V, Montes AH, Meana A, Celada A, Valle-Garay E.** Autoregulation mechanism of human neutrophil apoptosis during bacterial infection. *Mol Immunol* 45: 2087–2096, 2008.
27. **Oka M, Fagan KA, Jones PL, McMurtry IF.** Therapeutic potential of RhoA/Rho kinase inhibitors in pulmonary hypertension. *Br J Pharmacol* 155: 444–454, 2008.
28. **Phillipson M, Kaur J, Colarusso P, Ballantyne CM, Kubes P.** Endothelial domes encapsulate adherent neutrophils and minimize increases in vascular permeability in paracellular and transcellular emigration. *PLoS ONE* 3: e1649, 2008.
29. **Pierce GF.** Inflammation in nonhealing diabetic wounds: the space-time continuum does matter. *Am J Pathol* 159: 399–403, 2001.
30. **Rumbaut RE, Harris NR, Sial AJ, Huxley VH, Granger DN.** Leakage responses to L-NAME differ with the fluorescent dye used to label albumin. *Am J Physiol Heart Circ Physiol* 276: H333–H339, 1999.
31. **Saito H, Minamiya Y, Kitamura M, Saito S, Enomoto K, Terada K, Ogawa J.** Endothelial myosin light chain kinase regulates neutrophil migration across human umbilical vein endothelial cell monolayer. *J Immunol* 161: 1533–1540, 1998.
32. **Seasholtz TM, Brown JH.** Rho signaling in vascular diseases. *Mol Interv* 4: 348–357, 2004.
33. **Serhan CN, Chiang N, Van Dyke TE.** Resolving inflammation: dual anti-inflammatory and pro-resolution lipid mediators. *Nat Rev Immunol* 8: 349–361, 2008.
34. **Shaw SK, Bamba PS, Perkins BN, Luscinskas FW.** Real-time imaging of vascular endothelial-cadherin during leukocyte transmigration across endothelium. *J Immunol* 167: 2323–2330, 2001.
35. **Singer AJ, Clark RA.** Cutaneous wound healing. *N Engl J Med* 341: 738–746, 1999.
36. **Sun H, Breslin JW, Zhu J, Yuan SY, Wu MH.** Rho and ROCK signaling in VEGF-induced microvascular endothelial hyperpermeability. *Microcirculation* 13: 237–247, 2006.

37. **Taherzadeh M, Das AK, Warren JB.** Nifedipine increases microvascular permeability via a direct local effect on postcapillary venules. *Am J Physiol Heart Circ Physiol* 275: H1388–H1394, 1998.
38. **Vandenbroucke E, Mehta D, Minshall R, Malik AB.** Regulation of endothelial junctional permeability. *Ann NY Acad Sci* 1123: 134–145, 2008.
39. **Van der Heyde HC, Gramaglia I, Sun G, Woods C.** Platelet depletion by anti-CD41 (alphaIIb) mAb injection early but not late in the course of disease protects against *Plasmodium berghei* pathogenesis by altering the levels of pathogenic cytokines. *Blood* 105: 1956–1963, 2005.
40. **Van Nieuw Amerongen GP, Draijer R, Vermeer MA, van Hinsbergh VW.** Transient and prolonged increase in endothelial permeability induced by histamine and thrombin: role of protein kinases, calcium, and RhoA. *Circ Res* 83: 1115–1123, 1998.
41. **Vestweber D.** Adhesion and signaling molecules controlling the transmigration of leukocytes through endothelium. *Immunol Rev* 218: 178–196, 2007.
42. **Weber C.** Novel mechanistic concepts for the control of leukocyte transmigration: specialization of integrins, chemokines, and junctional molecules. *J Mol Med* 81: 4–19, 2003.
43. **Wedmore CV, Williams TJ.** Control of vascular permeability by polymorphonuclear leukocytes in inflammation. *Nature* 289: 646–650, 1981.
44. **Wojciak-Stothard B, Ridley AJ.** Rho GTPases and the regulation of endothelial permeability. *Vascul Pharmacol* 39: 187–199, 2002.
45. **Wojciak-Stothard B, Tsang LY, Paleolog E, Hall SM, Haworth SG.** Rac1 and RhoA as regulators of endothelial phenotype and barrier function in hypoxia-induced neonatal pulmonary hypertension. *Am J Physiol Lung Cell Mol Physiol* 290: L1173–L1182, 2006.
46. **Yoshinaga K, Inoue H, Tanaka F, Mimori K, Utsunomiya T, Mori M.** Platelet-derived endothelial cell growth factor mediates Rho-associated coiled-coil domain kinase messenger RNA expression and promotes cell motility. *Ann Surg Oncol* 10: 582–587, 2003.
47. **Yuan SY, Wu MH, Ustinova EE, Guo M, Tinsley JH, De Lanerolle P, Xu W.** Myosin light chain phosphorylation in neutrophil-stimulated coronary microvascular leakage. *Circ Res* 90: 1214–1221, 2002.
48. **Zeng L, Xu H, Chew TL, Eng E, Sadeghi MM, Adler S, Kanwar YS, Danesh FR.** HMG CoA reductase inhibition modulates VEGF-induced endothelial cell hyperpermeability by preventing RhoA activation and myosin regulatory light chain phosphorylation. *FASEB J* 19: 1845–1847, 2005.
49. **Zhu L, He P.** fMLP-stimulated release of reactive oxygen species from adherent leukocytes increases microvessel permeability. *Am J Physiol Heart Circ Physiol* 290: H365–H372, 2006.